AGU PUBLICATIONS

Journal of Advances in Modeling Earth Systems

RESEARCH ARTICLE
10.1002/2014MS000382

Improving a global model from the boundary layer: Total turbulent energy and the neutral limit Prandtl number

Felix Pithan[1,2,3], Wayne Angevine[4], and Thorsten Mauritsen[1]

[1]Max Planck Institute for Meteorology, Hamburg, Germany, [2]International Max Planck Research School for Earth System Sciences, Hamburg, Germany, [3]Now at Department of Meteorology, University of Reading, Reading, UK, [4]NOAA ESRL, Boulder, Colorado, USA

Key Points:
- A TTE closure improves the representation of turbulence in a GCM
- Reducing the turbulent Prandtl number affects modeled climate

Correspondence to:
F. Pithan,
f.pithan@reading.ac.uk

Citation:
Pithan, F., W. Angevine, and T. Mauritsen (2015), Improving a global model from the boundary layer: Total turbulent energy and the neutral limit Prandtl number, *J. Adv. Model. Earth Syst.*, *7*, 791–805, doi:10.1002/2014MS000382.

Received 5 SEP 2014
Accepted 4 MAY 2015
Accepted article online 6 MAY 2015
Published online 31 MAY 2015

Abstract Model intercomparisons have identified important deficits in the representation of the stable boundary layer by turbulence parametrizations used in current weather and climate models. However, detrimental impacts of more realistic schemes on the large-scale flow have hindered progress in this area. Here we implement a total turbulent energy scheme into the climate model ECHAM6. The total turbulent energy scheme considers the effects of Earth's rotation and static stability on the turbulence length scale. In contrast to the previously used turbulence scheme, the TTE scheme also implicitly represents entrainment flux in a dry convective boundary layer. Reducing the previously exaggerated surface drag in stable boundary layers indeed causes an increase in southern hemispheric zonal winds and large-scale pressure gradients beyond observed values. These biases can be largely removed by increasing the parametrized orographic drag. Reducing the neutral limit turbulent Prandtl number warms and moistens low-latitude boundary layers and acts to reduce longstanding radiation biases in the stratocumulus regions, the Southern Ocean and the equatorial cold tongue that are common to many climate models.

1. Introduction

Turbulent motion on scales from a few metres to the depth of the planetary boundary layer cannot be resolved in general circulation models (GCMs) with a horizontal grid spacing ranging from a few to about a hundred kilometres. Global atmospheric models that resolve deep convection are at the horizon of technical capabilities [*Satoh et al*., 2008], but boundary-layer turbulence will remain unresolved in global models for the foreseeable future.

Horizontal turbulent fluxes of momentum, heat, moisture or other tracers are usually negligible at the resolution of current GCMs, but vertical turbulent fluxes are crucial and thus need to be parametrized. The task of a turbulence parametrization is to predict the mean turbulent fluxes in the vertical for given profiles of wind and buoyancy, the latter being a function of temperature and moisture. Any set of equations that can be derived from first principles of physics to describe turbulent fluxes contains more unknowns than equations and thus cannot be solved; a problem known as the turbulence closure problem. Empirical relationships or turbulence closures are therefore needed to parametrize turbulent fluxes for weather and climate models. The GABLS (Global Atmospheric Boundary Layer Studies) model intercomparisons have shown that the turbulence schemes used in operational models still struggle to represent stable boundary layers (SBL) and the diurnal cycle of near-surface variables, with many models overestimating diffusivity under stable stratification [*Cuxart et al*., 2006; *Holtslag et al*., 2013].

Surface drag generates ageostrophic flow in the boundary layer and thereby plays an important role in controlling large-scale pressure gradients. The more surface drag a turbulence scheme produces for a given geostrophic wind, the more ageostrophic flow is generated in the boundary layer [*Svensson and Holtslag*, 2009], dampening synoptic systems. For cyclones, this dampening occurs through stress-induced Ekman-pumping [*Beare*, 2007] and the generation of potential vorticity (PV), which acts to increase stability above the low centre and thus reduces the influence of the upper-level PV anomaly on the near-surface flow [*Boutle et al*., 2015]. Enhanced damping from exaggerated turbulent diffusivities is known to improve the performance of numerical weather prediction models [*Viterbo et al*., 1999]. Reducing stable boundary-layer diffusivity to more realistic values leads to overly strong high and low-pressure systems in ECMWF model

forecasts, but changes to the orographic drag schemes can at least partly compensate for these deteriorations [*Sandu et al*., 2013].

The representation of boundary-layer processes in general circulation models also affects the thermodynamical aspects of climate. The behavior of low-level clouds in a warming climate, for example, has repeatedly been identified as a key uncertainty in determining the warming caused by a given increase in greenhouse gases [e.g., *Bony et al*., 2006]. We here address two aspects of boundary-layer turbulence that matter for thermodynamical aspects of the modeled climate, the ratio of turbulent diffusivity for momentum to diffusivity for heat known as the Prandtl number and the representation of entrainment in dry convective boundary layers. The near-surface gradients of temperature and humidity directly depend on the Prandtl number in the surface layer, but the consequences of assuming a specific Prandtl number are rarely discussed in the context of weather and climate modeling. In fact, many models implicitly assume a neutral limit Prandtl number Pr_0 of unity in the surface layer [*Liu et al*., 2013], whereas published estimates for Pr_0 range between 0.7 and unity [*Kays*, 1994]. Since the neutral limit Prandtl number is a potentially important parameter used in climate models and its value is controversial, we believe that the sensitivity of model results to choices of that parameter should be assessed.

The present paper documents the implementation of a total turbulent energy (TTE) scheme [*Mauritsen et al*., 2007; *Angevine et al*., 2010] into the climate model ECHAM6 [*Stevens et al*., 2013] and investigates how changes in the representation of boundary-layer processes impact the modeled climate. In contrast to the previously used turbulent kinetic energy scheme, the TTE scheme uses observationally based stability functions for the stable boundary layer and a turbulent length scale for the convective boundary layer that takes into account the distance to the capping inversion. It therefore yields a more realistic representation of stable boundary layers and of entrainment mixing at the capping inversion of dry convective boundary layers. We further investigate how reducing the ratio between the eddy diffusivities for momentum and heat, the Prandtl number $Pr = \frac{K_m}{K_h}$, affects the modeled climate.

We set off by reviewing some theoretical foundations of boundary-layer parametrizations to introduce the turbulent kinetic energy scheme currently used in ECHAM and the total turbulent energy scheme implemented for this study. We then describe the climate model itself, the experiments and data sets used (Section 3) and investigate the effect of reduced surface drag in single-column and global experiments. Finally, we investigate the impact of the TTE scheme and changes in the turbulent Prandtl number on thermodynamic aspects of the modeled climate.

2. From Turbulent Kinetic to Total Turbulent Energy

2.1. Theoretical Foundations of Turbulence Parametrizations

Following Prandtl's mixing length concept [*Prandtl*, 1925] and assuming a mixing length of $l = \kappa z$ in the surface layer, where κ is the von Kármán constant and z the height above the surface, the momentum flux in the surface layer is given as

$$\overline{u'w'} = -(\kappa z)^2 \left|\frac{\partial U}{\partial z}\right| \frac{\partial U}{\partial z}. \tag{1}$$

Taking the square root of (1), we obtain

$$\frac{\partial U}{\partial z} = \frac{u_*}{\kappa z}, \tag{2}$$

which can be integrated to yield the logarithmic wind profile. Rearranging and elevating to the power of two yields

$$\overline{u'w'} = u_*^2 = \frac{\kappa^2}{\ln^2\left(\frac{z}{z_0}\right)} U(z), \tag{3}$$

which is used to parametrize the surface momentum flux based on the first-level wind in many models. In the above equations, the coordinate system is assumed to be aligned with the mean wind U, overbars

denote time means, primes deviations from the mean, and z_0 is the aerodynamic roughness length, defined as the height above the surface at which the logarithmic wind profile vanishes.

Near the neutral limit, the heat flux can be derived in an analogous way using the ratio of turbulent diffusivity for heat to that for momentum called the turbulent Prandtl number, $Pr = \frac{K_m}{K_h}$:

$$\overline{w'\theta'} = -\frac{1}{Pr}\kappa^2 z^2 \left|\frac{\partial U}{\partial z}\right| \frac{\partial \theta}{\partial z} \tag{4}$$

Dividing by the friction velocity, defining $\theta_* = -\frac{\overline{w'\theta'}}{u_*}$ and rearranging yields

$$\frac{\partial \theta}{\partial z} = Pr \frac{\theta_*}{kz}, \tag{5}$$

To account for the effect of stable or unstable stratification, the fluxes obtained from equations (3) and the corresponding equation for heat flux are further scaled with empirically derived stability functions $f_{m,h}(Ri)$, where the Richardson number Ri is the ratio of stratification to wind shear and thus a measure of stability [*Louis*, 1979; *Mauritsen and Svensson*, 2007]. We will later discuss the crucial role these stability functions play for modeling stable boundary layers. Note how a larger Prandtl number will yield stronger temperature gradients in the surface layer (equation (5)). We will return to how this can affect global climate.

Many turbulence parametrizations describe turbulence in the atmosphere as a diffusive process generating a downgradient flux of a quantity X

$$F_X = -K \frac{\partial X}{\partial z}, \tag{6}$$

where K is the eddy diffusivity. In so-called first order closures, K is determined directly from the mean quantities such as the mean wind velocities at each level. 1.5-order or turbulent kinetic energy (TKE) closures use one further prognostic variable to describe the second moments of velocity, the turbulent kinetic energy.

In the context of atmospheric modeling, a problematic property of the TKE scheme is the existence of a critical Richardson number Ri_{crit}, a stability beyond which turbulence cannot be sustained and the flow becomes laminar [*Richardson*, 1920]. This threshold can be derived from the TKE budget equation

$$\frac{DE_{kin}}{Dt} = \tau \cdot S + \frac{g}{\theta}\overline{w'\theta'} - \gamma - \frac{\partial F_E}{\partial z}, \tag{7}$$

where the first term on the right-hand side is referred to as shear production of turbulence, the second term as buoyancy production under unstable or buoyancy destruction under stable stratification, and the remaining terms represent dissipation and the divergence of the turbulent flux of turbulent energy. Beyond the critical Richardson number, buoyancy destruction exceeds shear production, turbulence cannot be sustained and the flow becomes laminar. However, observational studies have shown turbulence to be present at very high stabilities [e.g., *Kondo et al.*, 1978; *Smedman*, 1988; *Mauritsen and Svensson*, 2007], and a breakdown of turbulence can cause both unphysical runaway cooling of the surface and numerical stability problems in models. To avoid such turbulence shutdowns, the stability functions $f_{m,h}(Ri)$ that were originally derived from observations have often been modified heuristically at the price of introducing artificially high diffusivities under stable stratification [*Louis*, 1979; *Viterbo et al.*, 1999]. A turbulence closure that avoids an implicit critical Richardson number by construction would thus be advantageous for the representation of stably stratified boundary layers in GCMs. We will show later how such a closure can be obtained by using total turbulent energy (TTE) rather than turbulent kinetic energy as prognostic variable.

We here give a brief description of the 1.5-order turbulence scheme currently used in ECHAM [*Brinkop and Roeckner*, 1995]. Turbulent diffusivity K_m and conductivity K_h are computed as

$$K_{m,h} = l \cdot f_{m,h} \cdot \sqrt{E_k}, \tag{8}$$

where l is the mixing length, $f_{m,h}$ are the stability functions for heat and momentum and E_k is turbulent kinetic energy. The mixing length l is obtained following *Blackadar* [1962]

$$\frac{1}{l} = \frac{1}{kz} + \frac{1}{\lambda}, \tag{9}$$

where λ equals 150 m in the boundary layer and decreases exponentially to 1 m in the free troposphere. Note that the neutral stability coefficients are different from unity and different for heat and momentum, leading to a neutral limit Prandtl number of about 0.8.

In the surface layer, drag coefficients are computed from the roughness lengths and stability functions based on *Louis* [1979] following the same concept as in equations (3) and the corresponding equation for heat. Roughness lengths over ocean are derived from the *Charnock* [1955] relation: $z_{0,m}=0.018u_*^2 * g^{-1}$ and $z_{0,h}=z_{0,m}exp\left(2-86.276z_{0,m}^{0.375}\right)$. Note that while earlier versions of ECHAM included effects of subgrid orography into the computation of roughness lengths over land, ECHAM6.2 only uses information about vegetation and snow cover.

The neutral limit turbulent Prandtl number was taken to be 0.74 in the original scheme by *Louis* [1979], but is considered to be unity in the scheme's current implementation in ECHAM. On the other hand, the roughness lengths for momentum z_0 and heat z_{0h} were identical in the original *Louis* [1979] scheme, whereas they can differ over ocean and to some extent over land in ECHAM6. For unstable conditions over ocean, the stability coefficient for heat f_h is computed using a free-convection approximation [*Miller et al*., 1992] to account for the mixing by convective eddies at low mean wind velocities. The effective ratio of the drag coefficients for momentum and heat over ocean is therefore no unique function of static stability.

2.2. Total Turbulent Energy Scheme

TTE is defined as the sum of turbulent kinetic energy and turbulent potential energy E_p [*Zilitinkevich et al*., 2007]

$$E_p=\frac{1}{2}\sigma_\theta^2\frac{\beta^2}{|N^2|}, \tag{10}$$

the equivalent of available potential energy. When an air parcel is displaced against the buoyancy gradient of a stable boundary layer, turbulent kinetic energy is destroyed in a TKE scheme. In a TTE scheme, TKE is instead converted to turbulent potential energy, and TTE is conserved. Total turbulent energy is only lost through dissipation, and can therefore be in a steady state at arbitrary stabilities.

We implement the TTE closure developed by *Mauritsen et al*. [2007] based on observations of stably stratified turbulence [*Mauritsen and Svensson*, 2007] with a turbulence length scale tuned to match a set of large-eddy simulations. A detailed description of the scheme and derivation of important quantities are given in *Mauritsen et al*. [2007], so we here limit ourselves to laying out key terms for the boundary-layer fluxes. *Angevine et al*. [2010] extended the TTE closure for use in unstable conditions when developing an eddy-diffusivity mass-flux scheme for the Weather Research and Forecast model (WRF). We use their developments for the eddy diffusivity component under unstable stratification but do not introduce the mass flux component, because convective mass flux is handled by the convection scheme in ECHAM6.

The budget equation for total turbulent energy can be obtained as the sum of the budget equations for turbulent kinetic and turbulent potential energy. It reads

$$\frac{DE}{Dt}=\tau\cdot S-\gamma-\frac{\partial F_E}{\partial z}+\begin{cases}0 & \text{for } N^2\geq 0\\ 2\beta\overline{w'\theta'} & \text{for } N^2<0\end{cases}, \tag{11}$$

where τ is the turbulent stress, S the wind shear, $\gamma=0.07E^{1.5}l^{-1}$ the dissipation rate, $\beta=g\theta^{-1}$ the buoyancy parameter, $N^2=\beta\frac{\partial\theta}{\partial z}$ the square of the Brunt-Vaisala frequency, $F_E=-|S|l^2\frac{\partial E}{\partial z}$ is the turbulent flux of turbulent energy and l the turbulence length scale. Again following *Mauritsen et al*. [2007] and *Angevine et al*. [2010], the ratio of turbulent potential to turbulent kinetic energy is diagnosed as

$$\frac{E_p}{E_k}=\begin{cases}\dfrac{Ri}{2\cdot Ri-Pr_0} & \text{for } Ri<0\\ \dfrac{Ri}{3\cdot Ri+Pr_0} & \text{for } Ri\geq 0,\end{cases} \tag{12}$$

which limits to $\frac{Ri}{Pr_0}$ as the Richardson number approaches zero.

Above the surface, the turbulent diffusivity (K_m) and conductivity (K_h) under stable stratification are computed as

$$K_m = \frac{f_\tau^2 E_k^2}{C_\epsilon \frac{E_k\sqrt{E}}{l_{stable}} - \beta f_\theta \sqrt{E_k \sigma_\theta^2}} \tag{13}$$

and

$$K_h = \frac{2 f_\theta^2 E_k l_{stable}}{C_\Phi \sqrt{E}}. \tag{14}$$

The respective coefficients under unstable stratification are obtained as

$$K_m = \frac{f_\tau^2}{C_\epsilon} l_{unstable} \sqrt{E_k} f_m(Ri) \tag{15}$$

and

$$K_h = Pr_0^{-1} K_m f_h(Ri) \tag{16}$$

with $C_\epsilon = C_\Phi = 0.07$. The computation of the lengths scales l_{stable} and $l_{unstable}$ will be explained below. For convective boundary layers, the unstable form of the diffusivity equations is used up to $z = 0.5 h_d$ and above if the resulting diffusivities exceed those from the stable form of the equations. Under stable conditions, the scheme uses observationally derived stability functions formulated in terms of the nondimensional stress $f_\tau = \frac{|\tau|}{E_k}$ and heat flux $f_\theta = \frac{\overline{w\theta}}{\sqrt{E_k \sigma_\theta^2}}$, where $f_\tau = 0.17\left(0.25 + 0.75(1+4Ri)^{-1}\right)$ and $f_\theta = -0.145(1+4Ri)^{-1}$ [*Mauritsen and Svensson*, 2007]. While *Angevine et al.* [2010] included mass-flux into their scheme and thus no longer required the use of empirical stability functions under unstable conditions, we here retain ECHAM's standard stability functions based on *Louis* [1979] for the unstable case.

The TTE scheme uses a turbulent length scale representing the size of the largest eddies, which determine the spatial scale of mixing processes and the dissipation of turbulent energy. Under stable stratification, eddies are limited in size by the distance to the surface, deformation by the Coriolis force and static stability. Implementing these constraints in ECHAM-TTE is a conceptual advance over the previous scheme, which only considered the distance to the surface and a fixed asymptotic length scale far away from the surface [*Blackadar*, 1962]. For convective boundary layers, an up-down length scale based on the distance to the surface and the dry thermal top is used. The length scale l is computed as

$$\frac{1}{l_{stable}} = \frac{1}{kz} + \frac{f}{C_f\sqrt{\tau}} + \frac{N}{C_N\sqrt{\tau}} \tag{17}$$

or

$$\frac{1}{l_{unstable}} = \frac{1}{kz} + \frac{3}{k(h_d - z)}, \tag{18}$$

where $f = 2\Omega$ is the Coriolis parameter, $C_f = 0.185$ and $C_N = 2$ are tunable parameters of the scheme, and h_d is the dry thermal top in a convective boundary layer, defined as the height where dry static energy equals that of the lowest model level. Outside the boundary layer, the same equations are applied, but the mixing length is not allowed to exceed 150 m to avoid numerical instabilities.

Surface fluxes are computed as

$$\tau = \frac{l^2}{(f_{sl}\cdot z_1)^2 \ln^2\left(\frac{z}{z_0}\right)} \frac{f_\tau(Ri)}{f_\tau(0)} (U^2 + V^2) \tag{19}$$

and

$$\overline{w'\theta'} = \frac{l^2}{(f_{sl}\cdot z_1)^2 \ln\left[\frac{z_1}{z_{0t}}\right] \ln\left[\frac{z_1}{z_{0m}}\right]} \frac{f_\theta(Ri)}{f_\theta(0)} \frac{1}{Pr_0} \sqrt{\frac{f_\tau(Ri)}{f_\tau(0)} \cdot (U^2 + V^2 + c_w w_*^2)} (\theta_1 - \theta_0), \tag{20}$$

where z_1 is the height of the first model level, usually around 30 m, $w_* = \left(g\theta_v^{-1} h_d \overline{w'\theta_v'}\right)^{1/3}$ is the convective velocity scale, c_w is the ratio of the mean absolute wind at the first level to the convective velocity scale

under free convection, and f_{sl} is the fraction of the first-level height at which the surface fluxes are nominally evaluated. Since computing the convective velocity scale w_* requires a priori knowledge of the turbulent heat flux, w_* from the last time step is used to compute the turbulent fluxes. Thereafter, w_* is updated following $w_* = 0.5(w_{*old} + w_{*new})$ to achieve numerical stability.

Note that *Mauritsen et al.* [2007] used $f_{sl} = 0.5$ and extrapolated fluxes from the next atmospheric flux level down to the surface. Implementing such an extrapolation in a GCM would be complicated due to the different surface properties that may be contained in one gridbox, and attempts to do so lead to numerical instability. To avoid such complications and keep the scheme reasonably simple, we revert to using the standard assumption of computing fluxes within the constant flux layer close to the surface. This leads to a slight reduction of surface drag in the GABLS1 case, for which we compensate by reducing the nominal height used for the flux computation, the parameter f_{sl}, from 0.5 to 0.4.

Following *Beljaars* [1994], we include the convective velocity scale into the total wind speed used to derive the surface heat flux in order to account for free convection (equation (20)). The ratio of the mean absolute wind at the first level to the convective velocity scale under free convection, c_w, was suggested to be 1.2 by *Beljaars* [1994], but shown to be around 0.5 in recent DNS experiments of a free-convective boundary layer [*Garcia and Mellado*, 2014].

The lower boundary condition for total turbulent energy is taken to be the steady state solution,

$$E = \left(1 + \frac{E_p}{E_k}\right) \cdot \frac{1}{f_\tau} \left(u_*^3 + l \cdot 2 \frac{g}{\theta_v} \overline{w'\theta'}\right)^{2/3}. \tag{21}$$

The computation of roughness lengths is the same as described above for ECHAM6.2.

3. Model, Data, and Experiments

3.1. ECHAM6 Climate Model

We use the atmospheric component of the MPI climate model ECHAM6. A new radiation scheme, a change of roughness length computation over land, and a number of bugfixes distinguish ECHAM 6.2.00 used here from version 6.1 used in the 5th phase of the Coupled Model Intercomparison Project (CMIP5) and documented by *Stevens et al.* [2013].

Surface drag by nonresolved orography is represented as a drag force opposed to the mean wind [*Lott*, 1999]. The mountain lift part of that scheme which generates a force perpendicular to the mean wind is not used in the standard version of ECHAM, but enabled for tuning ECHAM-TTE after implementing a modification described in Appendix A.

The prognostic equation for turbulent kinetic or total turbulent energy is solved implicitly [*Brinkop and Roeckner*, 1995]. Vertical fluxes of heat, momentum and tracers including surface fluxes are computed using an integrated implicit solver [*Schulz et al.*, 2001]. Surface fluxes, 2 m temperatures and 10 m winds are diagnosed following *Geleyn* [1988].

ECHAM uses a staggered vertical coordinate, where temperature, moisture and wind velocities are computed at full levels, whereas turbulent energy and the fluxes of heat, moisture and momentum are defined at half levels. The lowest half level is located at the surface, and in the standard vertical resolution with 47 levels, the lowest full level is located about 30 m above the ground. The next full level is placed at around 120 m and a total of about ten levels represent the lowermost 3 km of the atmosphere. Past increases in the number of levels have primarily served to improve the representation of the stratosphere, such that the vertical resolution in the boundary layer is identical for past and current versions of ECHAM using 31,47 and 95 levels. Standard model runs are made using version 6.2.00 and ECHAM-TTE corresponds to revision 3588 (echam_6.2.00_tte_fxp).

3.2. Data

ERA-Interim reanalysis data [*Simmons et al.*, 2007] are used to evaluate the performance of the different versions of ECHAM. The reanalysis is obtained by assimilating a large array of observations into the ECMWF model. Especially in regions with few or no regular observations, the reanalysis is model dependent and should thus be interpreted with caution. Results from direct numerical simulations of a free convective boundary layer [*Garcia and Mellado*, 2014] and from large-eddy simulations of a moderately stable boundary layer [*Beare et al.*, 2006] are used to evaluate the single-column experiments.

Table 1. Setup of the Single-Column Experiments[a]

Experiment	SBL (GABLS1)	dry CBL
z_{0m}, z_{0h}	0.1 m	0.1 m
$T(0)_{initial}$	265 K	290 K
$\frac{dT(0)}{dt}$	-0.25 Kh^{-1}	0.5 Kh^{-1}
$T(z)_{initial}$	$\theta = \begin{cases} 265\text{ K} & ,z \le 100\text{ m} \\ 265\text{ K} + 0.01\text{ Km}^{-1} \cdot z & ,z > 100\text{ m} \end{cases}$	T = 290 K + 0.0065 Km^{-1} · z
ugeo	8 ms^{-1}	0 or 10 ms^{-1}
latitude	73°N	50°N

[a]Radiation schemes are switched off, and latent heat fluxes and atmospheric moisture are set to zero in both cases. u_{geo} is the geostrophic wind.

3.3. Experiments

We run the global model with prescribed sea-surface temperatures and sea-ice concentrations as observed from 1979 to 2008 (AMIP setup). For the stable boundary layer single-column experiments, we use the GABLS1 setup [*Cuxart et al.*, 2006], where prescribed surface cooling (0.25 Kh^{-1}) and a constant geostrophic wind (8 ms^{-1}) drive the development of a moderately stable boundary layer. For the unstable case, we use a similar setup with prescribed surface warming (0.5 Kh^{-1}), a linear initial temperature profile and geostrophic winds of 0 and 10 ms^{-1} (Table 1).

4. Results and Discussion

We use the experiments described in section 3 to test whether the implementation of the total turbulent energy scheme has indeed improved the represenation of surface drag in stably stratified boundary layers, how it affects the large-scale flow and whether we can tune the model to compensate for any detrimental effects of reduced surface drag on circulation. We further investigate if the new mixing formulation for dry convective boundary layers yields the expected improvement of entrainment flux and how changes in the Prandtl number affect boundary-layer properties and TOA radiation balance.

4.1. Surface Drag in Stable Boundary Layers and the Large-Scale Circulation

ECHAM 6.2 produces too much surface drag in stable boundary layers, as do many operational models (Figure 1). For a shear-driven moderately stable boundary layer, the friction velocity from ECHAM 6.2 is outside the range of LES results and close to the most diffusive models in the GABLS1 intercomparison [*Cuxart et al.*, 2006]. The TTE scheme produces more realistic results in the middle of the LES range. Surface drag can be varied by changing the fraction of the first-level height at which surface fluxes are nominally evaluated (f_{sl}). As mentioned in the description of the TTE scheme, we reduce f_{sl} from 0.5 to 0.4 to compensate for the lack of flux interpolation in ECHAM. The original implementation of the TTE-scheme from *Mauritsen et al.* [2007] into a standalone-Matlab model uses a much higher vertical resolution and interpolates fluxes from the lowest flux level to the surface. When run at a similar resolution as ECHAM, the original implementation produces somewhat lower surface drag with friction within the lower part of the LES range (not shown).

Prior studies have shown that reduced, more realistic surface drag in stable boundary layers is often detrimental to the representation of the large-scale flow in global models [e.g., *Viterbo et al.*, 1999; *Sandu et al.*, 2013]. Implementing the total turbulent energy scheme without substantially worsening the model's performance in regard of mean sea-level pressure and zonal mean zonal wind velocities would therefore already be a success. In comparison to the ERA-Interim reanalysis (Figure 2, top), the reference model version ECHAM 6.2 has an Azores high that is too strong and a low-pressure bias extending eastward from Iceland, which results in an exaggerated meridional pressure gradient over the North Atlantic. Further notable pressure biases include a high-pressure bias over the Northern Pacific and a low-pressure bias at the equatorward edge of the southern hemispheric storm track. ECHAM 6.2 also overestimates the zonal wind velocities in the extratropical

Table 2. Values of Tuning Parameters Changed Between ECHAM 6.2 and ECHAM-TTE

Tuning Parameter	Entrainment Rate for Shallow Convection (entrscv)	Subgrid-Scale Orographic Drag (gkdrag)	Subgrid-Scale Orographic Lift (gklift)
value in ECHAM 6.2	$3 \cdot 10^{-4}$ m^{-1}	0.2	0
value in ECHAM-TTE	$6 \cdot 10^{-4}$ m^{-1}	1.2	0.7

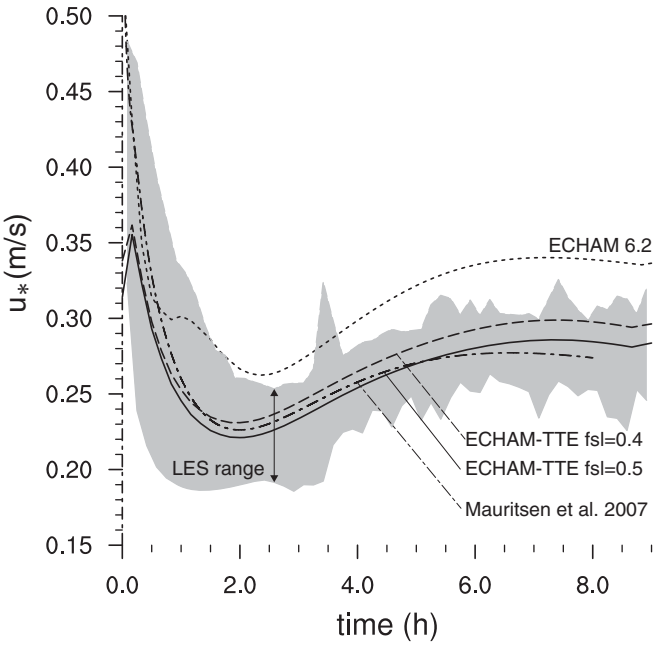

Figure 1. Friction velocity for the GABLS1 case. The gray shaded area denotes the range of LES results at 6.25 m resolution, the lines correspond to the original implementation of the TTE scheme as a standalone Matlab model by *Mauritsen et al.* [2007] (dash-dotted), ECHAM6.2 (short dashes), and ECHAM-TTE with $f_{sl} = 0.5$ (solid line) and 0.4 (dashed line). All ECHAM versions are run at the standard vertical resolution L47.

jetstreams (difference plots from ERA-Interim in the second row of Figure 2).

Running ECHAM-TTE without retuning any parameters leads a substantial overestimation of wind velocities and pressure gradients in the Southern hemisphere, whereas biases in the Nothern hemisphere are comparable to the standard version of ECHAM 6.2 (third row of Figure 2). In the Southern hemisphere, the model response to reduced surface drag is consistent with our physical understanding: Less surface drag leads to reduced cross-isobaric flow [*Svensson and Holtslag* 2009], which causes stronger synoptic activity. Both the resulting stronger pressure gradients and the reduced drag itself contribute to stronger zonal winds. In the Northern hemisphere, the reduced upper tropospheric wind biases in ECHAM-TTE are probably associated with the reduced temperature biases in the extratropical upper troposphere-lower stratosphere discussed in more detail in section 4.2 rather than changes in surface drag. To further alleviate the wind and pressure biases, we turn to the parametrization of subgrid-scale orographic drag [*Lott*, 1999] following *Sandu et al.* [2013].

In a first step, the tuning parameter for drag by orographically blocked flow is increased from 0.2 to 1.2 (C_d from equation (2) in *Lott* [1999], gkdrag in Table 2 of the present paper). This reduces zonal wind velocities especially in the jet regions and alleviates the biases in mean sea-level pressure (fourth row of Figure 2). However, the parameter change introduces a new high-pressure bias in the Arctic. We therefore activate the parametrization for mountain lift caused by subgrid-scale orography after implementing a modification described in Appendix A. Increasing C_l from equation (5) in *Lott* [1999] from zero to 0.7 largely removes the Arctic high-pressure bias. The parametrization for drag caused by orographically blocked flow [*Lott*, 1999] was also used to partly compensate for the overestimation of synoptic and planetary-scale activity in the reduced-diffusivity ECMWF model [*Sandu et al.*, 2013]. In that study, increasing turbulent orographic form drag [*Beljaars et al.*, 2004] compensated for the circulation biases more efficiently. Turbulent orographic form drag is however not implemented in ECHAM, so that we could not easily test its effect.

Both *Sandu et al.* [2013] and the present work suggest that the circulation biases that appear when surface drag is reduced to realistic values can be compensated to a substantial degree by retuning parts of the model related to effects of nonresolved orography. However, as was the case in ECHAM6.2, a tradeoff appears to exist between optimizing the circulation in either the Northern or the Southern hemisphere.

4.2. Entrainment Flux and Prandtl Number in Convective Boundary Layers and Thermodynamic Aspects of Climate

In a growing convective boundary layer, buoyant plumes from the convective layer penetrate into the capping inversion, generating a counterflow of warmer air into the boundary layer and thus causing a downward heat flux at the inversion, the entrainment flux.

Direct numerical simulations of the entrainment zone at the top of a growing boundary layer show a complex interplay between length scales and turbulence properties set by the convective plumes penetrating into the inversion as well as by the local stability [*Garcia and Mellado*, 2014]. At the lower end of the capping

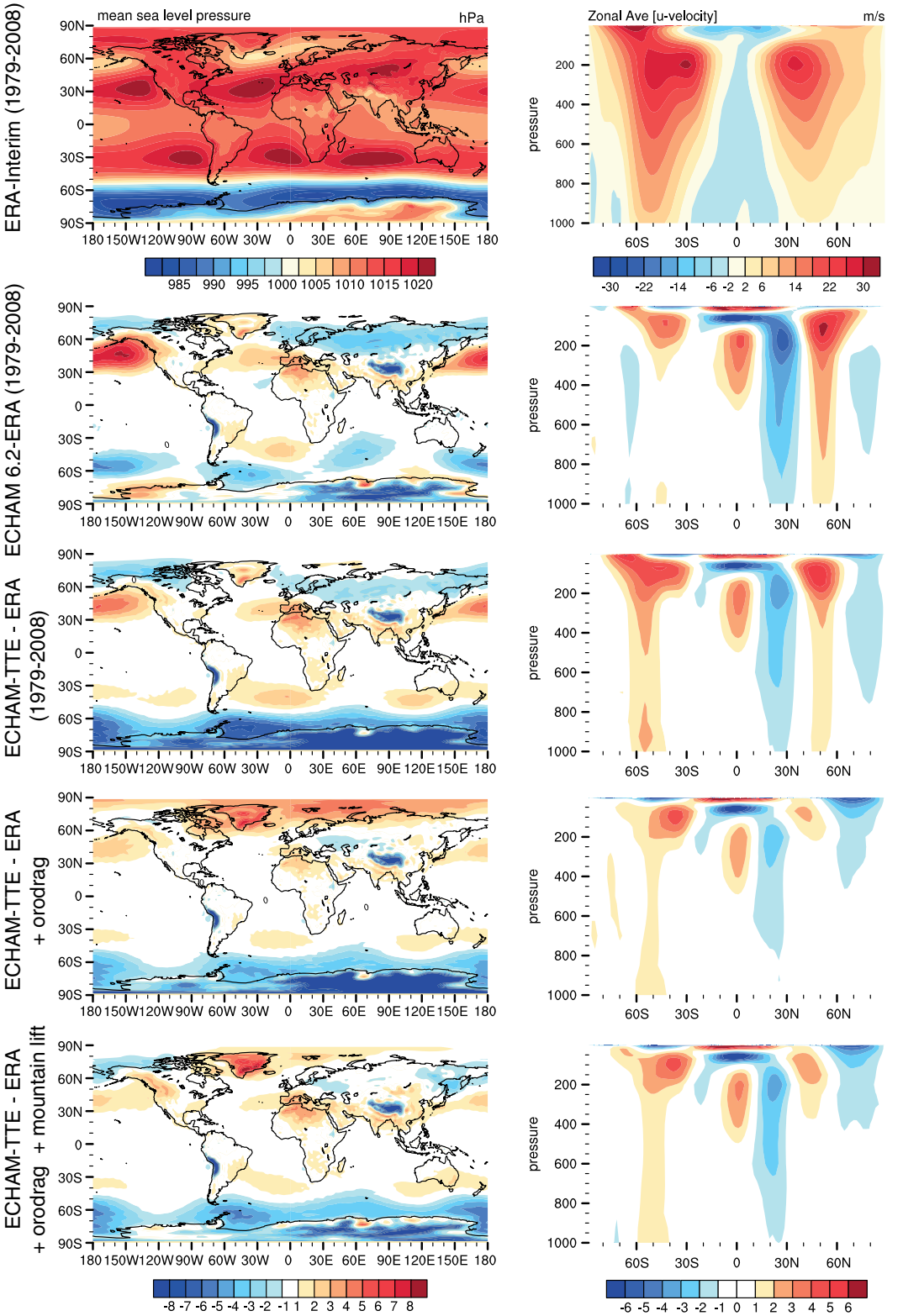

Figure 2. (left) Annual mean sea-level pressure fields and (right) zonal mean zonal winds for 1979–2008. Top plots show ERA-interim data, and the following rows the deviation of AMIP runs from the reanalysis (in hPa and m/s) when using ECHAM6.2, ECHAM-TTE without further tuning, ECHAM-TTE with enhanced orographic drag (+orodrag) and ECHAM-TTE with enhanced orographic drag and activated mountain lift scheme (+orodrag + mountain lift).

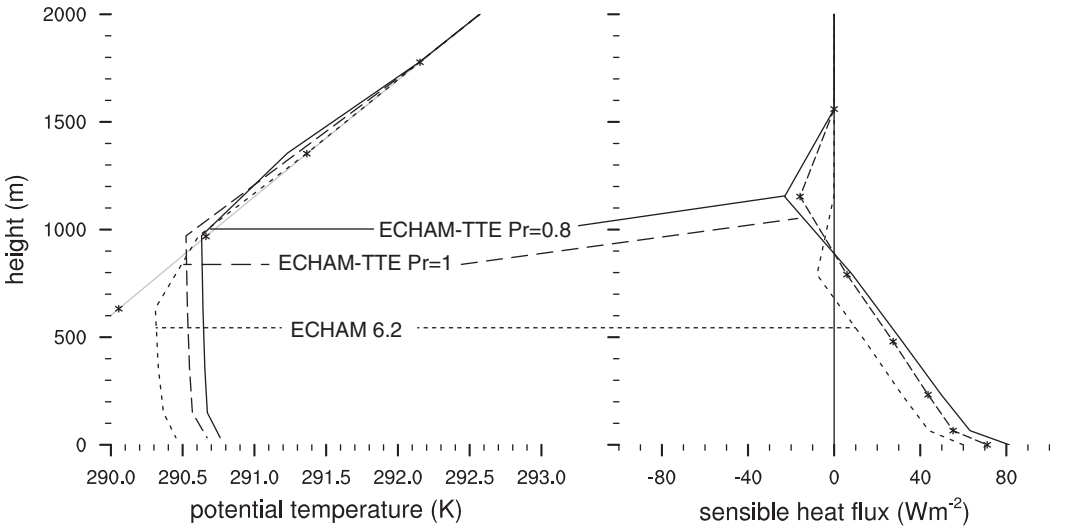

Figure 3. (left) Potential temperature and (right) sensible heat flux profiles for an idealized dry convective boundary-layer case with prescribed surface heating (u_{geo}=10 ms^{-1}) averaged over 1 h after 6 h of model integration. Results are from the single-column model using ECHAM6.2 and ECHAM-TTE, using neutral limit Prandtl numbers of 1 and 0.8 in ECHAM-TTE.

layer, the dominant length scale is the depth of the boundary layer, whereas further inside the capping layer, the length scale transitions to a scale proportional to the ratio of the convective velocity scale to the stratification, $\frac{w_*}{N}$. The standard version of ECHAM6 produces hardly any entrainment flux at the top of a growing CBL, such that no effect of entrainment on the evolution of the potential temperature profile is visible (Figure 3). A lack of entrainment mixing in stratocumulus-topped boundary layer was already noted for ECHAM4 [*Lenderink et al*., 2000]. ECHAM-TTE in contrast produces an entrainment flux that visibly affects the structure of the growing convective boundary layer and its capping inversion. Higher rates of entrainment in the new turbulence scheme are mostly achieved by using the convective length scale and diffusivities up to the dry thermal top whenever they are greater than the length scale and diffusivity obtained from the equations for stable stratification. The old scheme is formulated purely in terms of the local stability and therefore ignores the influence of the underlying convective boundary layer at the first flux level within the capping inversion, treating this level as part of the stable free troposphere (Figure 4b). This leads to turbulence shutdown and absence of entrainment mixing. The new scheme effectively treats the entrainment zone or capping layer as a special part of the convective boundary layer (Figure 4c). Entrainment flux is implicitly computed in the turbulence scheme, i.e., without using an explicit entrainment parametrization that other models rely on, and results from the single-column model are comparable to those from direct numerical simulation for an idealized free-convective case (bottom row of Figure 4).

In contrast to the DNS profile, ECHAM maintains an unstable profile throughout the boundary layer both with the old and new turbulence scheme since it does not include a counter-gradient or mass-flux term (Figure 4). Note also that the sensible heat flux is not linear as one would expect, especially between the atmospheric and surface flux.

Coming back to the impact of the neutral limit Prandtl number on temperature profiles (equation (5)), we reduce the neutral turbulent Prandtl number in the surface layer. A lower neutral limit turbulent Prandtl number leads to a warmer convective boundary layer (Figure 3), as the resulting larger turbulent conductivity for heat reduces the temperature gradient between the surface and the first model level consistent with equation (5).

We now analyze the effect of the TTE scheme and changes in the Prandtl number on global model experiments (Figure 5). The most important temperature biases in ECHAM 6.2 are a widespread warm bias in near-surface air temperature over land, especially in the Northern Hemisphere, and a cold bias in the upper troposphere (second row in Figure 5). In ECHAM-TTE with a Prandtl number of 1, the extratropical cold biases in the upper troposphere/lower stratosphere are strongly alleviated in the Northern and somewhat reduced in the Southern hemisphere, whereas the tropical upper tropospheric cold bias becomes stronger

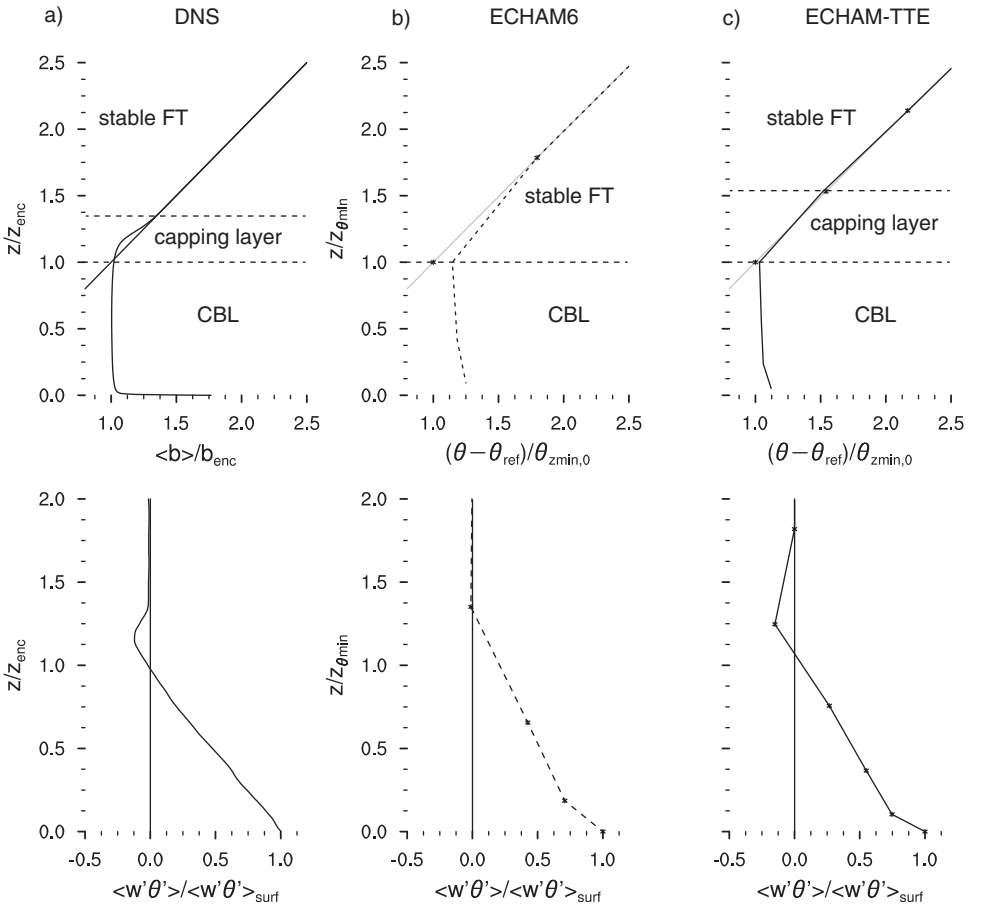

Figure 4. (top) Normalized buoyancy/potential temperature profiles and (bottom) sensible heat flux profiles of a growing dry free convective boundary layer. The DNS experiment is described in *Garcia and Mellado* [2014]. SCM experiments are normalized using the height of the minimum potential temperature as upper end of the mixed layer and a reference temperature of 290 K, which corresponds to the initial surface temperature of the background profile. DNS profiles are normalized using the encroachment height and buoyancy at that level (see *Garcia and Mellado* [2014]) for further details).

(third row in Figure 5). Reducing the turbulent Prandtl number, i.e., increasing the ratio of heat to momentum flux causes a warming especially of the tropical and subtropical boundary layers. As deep convective mixing leads to a near-constant lapse rate in the tropical troposphere, this warming is also communicated to the upper tropical troposphere (fourth row in Figure 5).

The reduced cold bias in the extratropical upper troposphere and lower stratosphere in ECHAM-TTE is consistent with the reduction of excessive westerlies at the same levels shown in the previous section, as an exaggerated meridional temperature gradient sustains a stronger thermal wind in ECHAM6.2.

The warming and deepening of the tropical and subtropical boundary layers caused by the new turbulence scheme is associated with a drying of the boundary layer and therefore a reduction in cloudiness. This causes a global TOA imbalance of several Wm^{-2}. To reduce the amount of absorbed shortwave radiation and achieve radiative balance at top-of-atmosphere [*Mauritsen et al.*, 2012], the entrainment rate for shallow convection in ECHAM-TTE is increased from $3 \cdot 10^{-4}$ to $6 \cdot 10^{-4}$ m^{-1}.

Reducing Pr_0 from 1 to 0.8 in ECHAM-TTE causes an increase in relative humidity in the boundary layer (Figure 6), reduced absorption of shortwave radiation in the stratocumulus regions and over the Southern ocean, where cloudiness is usually underestimated, and increased shortwave absorption over the equatorial pacific, which is often cold-biased in coupled climate models [*Wang et al.*, 2014]. Reducing the neutral limit Prandtl number from unity within the range of values suggested in the literature thus works against longstanding biases that are present in many climate models. However, smaller values of Pr_0 also result in high biases in atmospheric water vapour and globally averaged precipitation compared to estimates based on satellite observations.

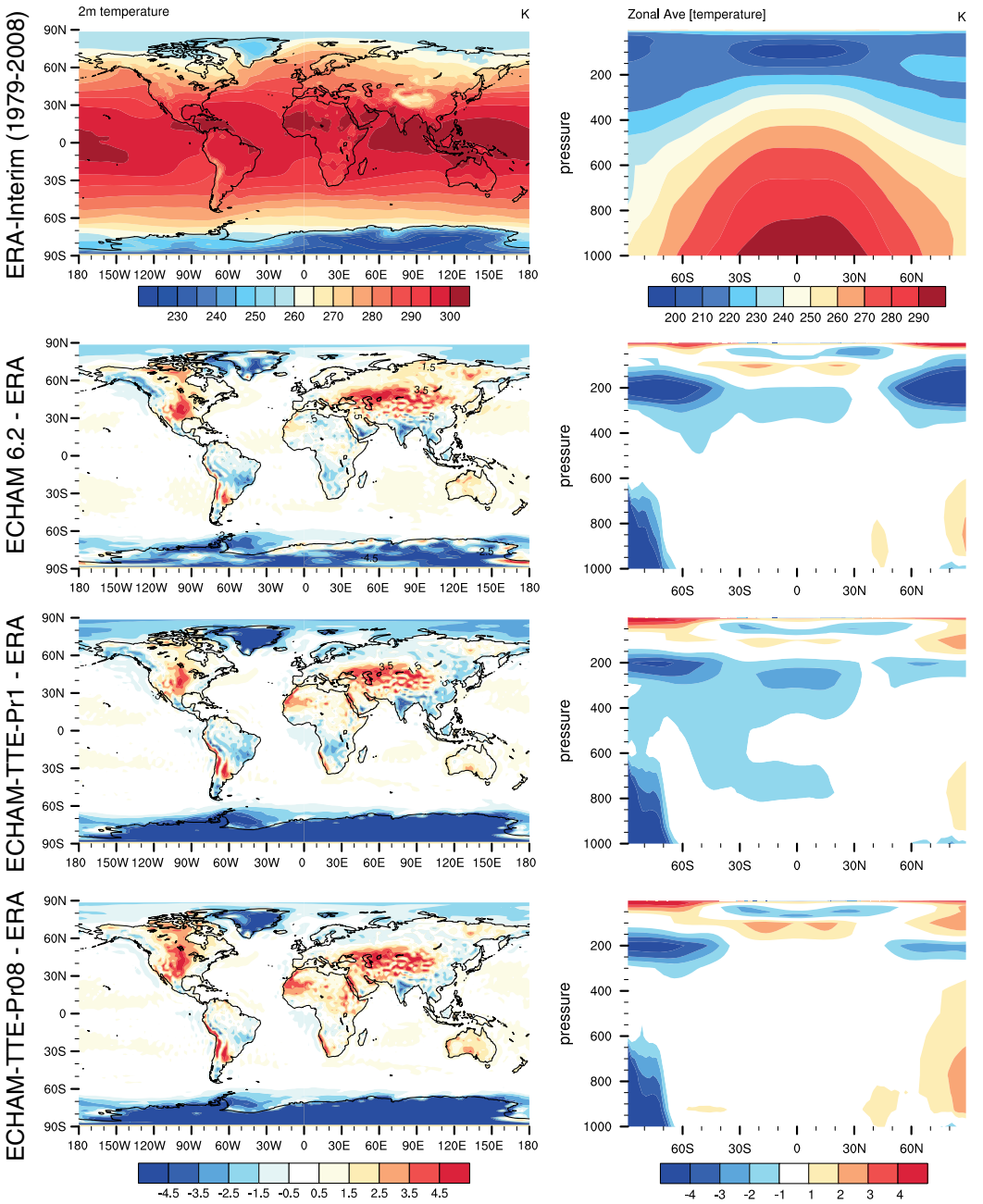

Figure 5. (left) Annual mean 2 m temperature and (right) zonal mean atmospheric temperature for ERA-Interim (top plots) and the difference of AMIP runs to reanalysis (in K) when using ECHAM6.2, ECHAM-TTE with a neutral-limit Prandtl number of 1 and ECHAM-TTE with a neutral limit Prandtl number of 0.8.

ECHAM uses different roughness lengths for heat and momentum over ocean, which could be thought of as representing the deviation of the Prandtl number from unity. However, setting these roughness lengths to an equal value hardly influences the variables that are affected by changes in the Prandtl number (not shown). Note that the model is evaluated against ERA-Interim, a reanalysis product derived using the IFS Cy31r1, which also assumes a neutral limit turbulent Prandtl number of one in the surface layer [*ECMWF*, 2007].

5. Summary

ECHAM6 overestimates diffusivity and thus surface drag in stably stratified boundary layers, as do many other climate and weather prediction models [*Cuxart et al.*, 2006]. We have implemented a new turbulence

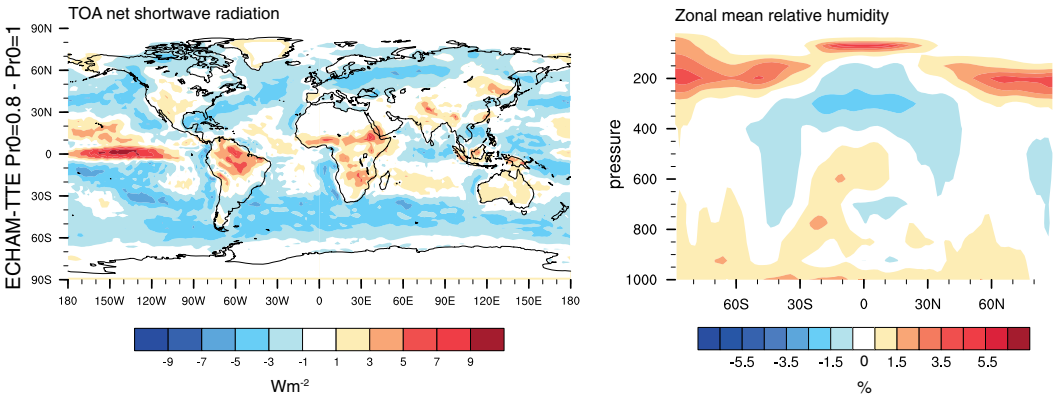

Figure 6. Annual mean changes in TOA net shortwave radiation and zonal mean relative humidity between ECHAM-TTE with Prandtl number $Pr_0 = 0.8$ and $Pr_0 = 1$ for an AMIP run (1979–2008).

scheme based on the concept of total turbulent energy [*Mauritsen et al*., 2007], which generates surface drag within the range of large-eddy simulations for an idealized moderately stable single-column case.

In the Southern hemisphere, reducing turbulent surface drag to realistic values leads to an unrealistic increase in large-scale pressure gradients and zonal wind speeds in agreement with our expectations and results from the ECMWF model [*Svensson and Holtslag*, 2009; *Sandu et al*., 2013]. These biases can largely be compensated for by increasing the parametrized drag caused by unresolved orography [*Lott*, 1999]. In the Northern hemisphere, the impact of reducing an upper-tropospheric cold bias with the new scheme appears to dominate over the effect of reduced surface drag, leading to a reduction of excessive upper tropospheric westerlies through the thermal wind balance.

Increasing drag from nonresolved orography is effective in compensating for the detrimental impacts of reduced surface drag on the large-scale circulation. However, a tradeoff remains between minimizing biases in either the Northern or Southern hemisphere. We conclude that further processes beyond turbulent surface drag and the effects of nonresolved orography need to be considered in order to obtain a realistic representation of the large-scale flow. A more detailed investigation of the tropospheric momentum budget from a surface perspective is necessary to understand the role of different sinks of momentum for the large-scale circulation.

The new scheme also includes an improved turbulence length scale for convective boundary layers and does generate entrainment fluxes at the top of a growing dry convective boundary layer comparable to results from direct numerical simulation [*Garcia and Mellado*, 2014], which the old turbulence scheme failed to achieve. The warming and deepening of marine boundary layers that results from an improved representation of entrainment flux is probably the cause for a reduced shortwave cloud radiative effect, which leads to an imbalance in top-of-atmosphere radiation. Increasing the entrainment rate for shallow convection largely compensates for this [*Mauritsen et al*., 2012]. Reducing the neutral turbulent Prandtl number, i.e., the ratio of eddy diffusivity for momentum to eddy conductivity for heat from unity to 0.8 leads an increase in relative humidity in the tropical and subtropical boundary layers. This works against typical climate model biases by reducing net shortwave flux in

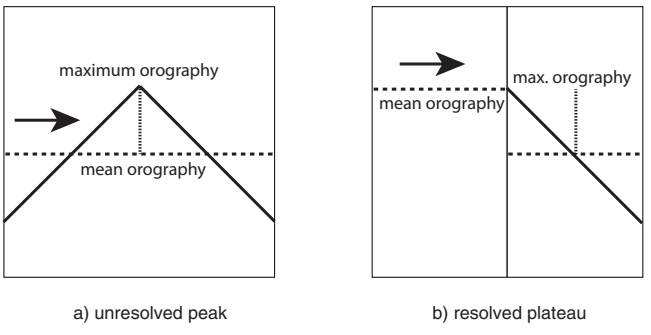

Figure 7. Sketch of the representation of nonresolved and resolved orographic features in the subgrid-scale orographic drag scheme. (a) The situation for which the scheme has been developed and (b) representative of the edges of large ice sheets, where the application of mountain lift forces to the difference between mean and maximum orography causes an unphysical spurious effect on the circulation which can cause substantial model biases.

the stratocumulus regions and over the Southern ocean, where models tend to absorb too much radiation, and increasing net shortwave flux over the equatorial cold tongue, where coupled models tend to be cold-biased [*Wang et al*., 2014]. The humidity difference between the boundary layer and the free troposphere at low latitudes is thought to play an important role in shaping low-level cloud feedbacks and thus climate sensitivity in models [*Sherwood et al*., 2014]. How the neutral limit turbulent Prandtl number affects the modeled climate and whether it affects cloud feedbacks and thus climate sensitivity should therefore be further investigated.

Improving the parametrization of atmospheric boundary-layer processes in climate models can yield substantial improvements in the model representation of important climate variables including the regional top-of-atmosphere radiation balance in areas of longstanding model biases. Compensating errors in different model components however pose a substantial challenge to the realization of such improvements. The concept of total turbulent energy allows the use of observationally based stability functions without risking unphysical turbulence breakdown at high stability, and with an improved formulation of the mixing length, the model implicitly computes realistic rates of entrainment flux in convective boundary layers.

Appendix A: Mountain Lift Parametrization

The subgrid orographic drag scheme by *Lott* [1999] represents the drag and mountain lift generated by nonresolved orography. The scheme computes a drag force opposed to the mean wind, which is thought to represent drag by orographically blocked flow, and a lift force perpendicular to the mean wind. However, the key tuning parameter for the lift parametrization is currently set to zero, such that only drag forces by the nonresolved orography are simulated. While alleviating some biases in the mean pressure fields, the mountain lift parametrization in its current implementation introduces new biases around Antarctica and in Northern Europe. We attribute these to a conceptual problem in the representation of the big ice sheets of Antarctica and Greenland, which have central plateaus resolved by the model grid (Figure 7). On the downwind side of the Greenland ice sheet and at the edges of the Antarctic plateau, the difference between the mean and the maximum orography therefore does not represent an unresolved peak. To remove this spurious effect, we modify the lift parametrization such that the largest resolved height of a gridpoint and all its immediate neighbours is considered the baseline which the maximum orography has to exceed. If the maximum exceeds this baseline, lift forces are computed based on the difference between the maximum and baseline orography.

Acknowledgments
We gratefully acknowledge Jade Garcia for sharing the DNS data used in this paper (documented in *Garcia and Mellado* [2014]) and her insights into surface and entrainment fluxes under free convection. ERA-Interim data were obtained from the ECMWF data server, LES data from the GABLS1 intercomparison were made available by *Beare et al*. [2006]. The ECHAM6 source code can be obtained from the MPI for Meteorology (http://www.mpimet.mpg.de/en/science/models/model-distribution.html). This work is part of the first author's dissertation at the University of Hamburg.

References

Angevine, W. M., H. Jiang, and T. Mauritsen (2010), Performance of an eddy diffusivity-mass flux scheme for shallow cumulus boundary layers, *Mon. Weather Rev.*, *138*(7), 2895–2912.
Beare, R. J. (2007), Boundary layer mechanisms in extratropical cyclones, *Q. J. R. Meteorol. Soc.*, *133*(623), 503–515.
Beare, R. J., et al. (2006), An intercomparison of large-eddy simulations of the stable boundary layer, *Boundary Layer Meterol.*, *118*(2), 247–272.
Beljaars, A. (1994), The parametrization of surface fluxes in large-scale models under free convection, *Q. J. R. Meterol. Soc.*, *121*(522), 255–270.
Beljaars, A., A. R. Brown, and N. Wood (2004), A new parametrization of turbulent orographic form drag, *Q. J. R. Meterol. Soc.*, *130*(599), 1327–1347.
Blackadar, A. K. (1962), The vertical distribution of wind and turbulent exchange in a neutral atmosphere, *J. Geophys. Res.*, *67*(8), 3095–3102.
Bony, S., et al. (2006), How well do we understand and evaluate climate change feedback processes?, *J. Clim.*, *19*(15), 3445–3482, doi: 10.1175/JCLI3819.1.
Boutle, I. A., S. E. Belcher, and R. S. Plant (2015), Friction in mid-latitude cyclones: An Ekman-pv mechanism, *Atmos. Sci. Lett.*, *16*, 103–109, doi:10.1002/asl2.526.
Brinkop, S., and E. Roeckner (1995), Sensitivity of a general circulation model to parameterizations of cloud–turbulence interactions in the atmospheric boundary layer, *Tellus, Ser. A*, *47*(2), 197–220.
Charnock, H. (1955), Wind stress on a water surface, *Q. J. R. Meteorol. Soc.*, *81*(350), 639–640.
Cuxart, J., et al. (2006), Single-column model intercomparison for a stably stratified atmospheric boundary layer, *Boundary Layer Meterol.*, *118*(2), 273–303.
ECMWF (2007), Ifs documentation—Cy31r1. Part IV: Physical processes, technical report, Reading, U. K.
Garcia, J. R., and J.-P. Mellado (2014), The two-layer structure of the entrainment zone in the convective boundary layer, *J. Atmos. Sci.*, *71*, 1935–1955, doi:10.1175/JAS-D-13-0148.1.
Geleyn, J.-F. (1988), Interpolation of wind, temperature and humidity values from model levels to the height of measurement, *Tellus, Ser., A*, *40*(4), 347–351
Holtslag, A., et al. (2013), Stable atmospheric boundary layers and diurnal cycles-challenges for weather and climate models, *Bull. Am. Meterol. Soc.*, *94*, 1691–1706.

Kays, W. M. (1994), Turbulent Prandtl number. Where are we?, *ASME Trans. J. Heat Transfer*, *116*, 284–295.
Kondo, J., O. Kanechika, and N. Yasuda (1978), Heat and momentum transfers under strong stability in the atmospheric surface layer, *J. Atmos. Sci.*, *35*(6), 1012–1021.
Lenderink, G., E. van Meijgaard, and A. A. Holtslag (2000), Evaluation of the ECHAM4 cloud-turbulence scheme for stratocumulus, *Meteorol. Z.*, *9*(1), 41–47.
Liu, G., Y. Liu, and S. Endo (2013), Evaluation of surface flux parameterizations with long-term arm observations, *Mon. Weather Rev.*, *141*(2), 773–797.
Lott, F. (1999), Alleviation of stationary biases in a GCM through a mountain drag parameterization scheme and a simple representation of mountain lift forces, *Mon. Weather Rev.*, *127*(5), 788–801.
Louis, J.-F. (1979), A parametric model of vertical eddy fluxes in the atmosphere, *Boundary Layer Meterol.*, *17*(2), 187–202.
Mauritsen, T., and G. Svensson (2007), Observations of stably stratified shear-driven atmospheric turbulence at low and high Richardson numbers, *J. Atmos. Sci.*, *64*(2), 645–655.
Mauritsen, T., G. Svensson, S. S. Zilitinkevich, I. Esau, L. Enger, and B. Grisogono (2007), A total turbulent energy closure model for neutrally and stably stratified atmospheric boundary layers, *J. Atmos. Sci.*, *64*(11), 4113–4126.
Mauritsen, T., et al. (2012), Tuning the climate of a global model, *J. Adv. Model. Earth Syst.*, *4*, M00A01, doi:10.1029/2012MS000154.
Miller, M., A. Beljaars, and T. Palmer (1992), The sensitivity of the ECMWF model to the parameterization of evaporation from the tropical oceans, *J. Clim.*, *5*(5), 418–434.
Prandtl, L. (1925), Bericht über Untersuchungen zur ausgebildeten Turbulenz, *Z. Angew. Math. Mech.*, *5*(2), 136–139.
Richardson, L. (1920), The supply of energy to and from atmospheric eddies, *Proc. R. Soc. London, Ser. A*, *97*(686), 354–373.
Sandu, I., A. Beljaars, P. Bechtold, T. Mauritsen, and G. Balsamo (2013), Why is it so difficult to represent stably stratified conditions in numerical weather prediction (NWP) models?, *J. Adv. Model. Earth Syst.*, *5*, 117–133, doi:10.1002/jame.20013.
Satoh, M., T. Matsuno, H. Tomita, H. Miura, T. Nasuno, and S. Iga (2008), Nonhydrostatic icosahedral atmospheric model (NICAM) for global cloud resolving simulations, *J. Comput. Phys.*, *227*(7), 3486–3514.
Schulz, J.-P., L. Dümenil, and J. Polcher (2001), On the land surface-atmosphere coupling and its impact in a single-column atmospheric model, *J. Appl. Meterol.*, *40*(3), 642–663.
Sherwood, S. C., S. Bony, and J.-L. Dufresne (2014), Spread in model climate sensitivity traced to atmospheric convective mixing, *Nature*, *505*(7481), 37–42.
Simmons, A., S. Uppala, D. Dee, and S. Kobayashi (2007), ERA-Interim: New ECMWF reanalysis products from 1989 onwards, *ECMWF Newsl.*, *110*, 25–35.
Smedman, A.-S. (1988), Observations of a multi-level turbulence structure in a very stable atmospheric boundary layer, *Boundary Layer Meterol.*, *44*(3), 231–253.
Stevens, B., et al. (2013), Atmospheric component of the MPI-M Earth System Model: ECHAM6, *J. Adv. Model. Earth Syst.*, *5*, 146–172, doi: 10.1002/jame.20015.
Svensson, G., and A. A. Holtslag (2009), Analysis of model results for the turning of the wind and related momentum fluxes in the stable boundary layer, *Boundary Layer Meterol.*, *132*(2), 261–277.
Viterbo, P., A. Beljaars, J.-F. Mahfouf, and J. Teixeira (1999), The representation of soil moisture freezing and its impact on the stable boundary layer, *Q. J. R. Meterol. Soc.*, *125*(559), 2401–2426.
Wang, C., L. Zhang, S.-K. Lee, L. Wu, and C. R. Mechoso (2014), A global perspective on CMIP5 climate model biases, *Nat. Clim. Change*, *4*(3), 201–205.
Zilitinkevich, S., T. Elperin, N. Kleeorin, and I. Rogachevskii (2007), Energy-and flux-budget (EFB) turbulence closure model for stably stratified flows. Part I: Steady-state, homogeneous regimes, *Boundary Layer Meterol.*, *125*(2), 167–191.